C. R. Mecanique 347 (2019) 455–462

Contents lists available at ScienceDirect

Comptes Rendus Mecanique

www.sciencedirect.com

Time reversal for obstacle location in elastodynamics from acoustic recording

Retournement temporel pour la localisation d'obstacles en élastodynamique à partir d'un enregistrement acoustique

Franck Assous *, Moshe Lin

Department of Mathematics, Ariel University, 40700 Ariel, Israel

ARTICLE INFO

Article history:
Received 4 December 2018
Accepted 4 February 2019
Available online 18 February 2019

Keywords:
Time reversal
Wave propagation
Inverse problem
Acousto-elastodynamics
Numerical simulation
Identification

Mots-clés :
Retournement temporel
Propagation d'ondes
Problèmes inverses
Acousto-élastodynamique
Simulation numérique
Identification

ABSTRACT

The Note is concerned with a feasibility study of time reversal in a non-homogeneous elastic medium, from data recorded in an acoustic medium. Our aim here is to determine the presence and some physical properties of elastic "inclusions" (unknown, not observable solid objects, characterized by their elastic properties) from partial observations of acoustic waves scattered by these inclusions. A finite element numerical method, based on a variational acousto-elastodynamics formulation, is derived and used to solve the forward, and then, the time-reversed problem. A criterion, derived from the reverse time migration framework, is introduced, to help construct images of the inclusions to be determined. Numerical illustrations on configurations that mimic the breast cancer configuration are proposed, and show that one can differentiate between two inclusions, even with different properties.

RÉSUMÉ

Le but de cette note est d'étudier le retourné temporel d'un problème posé dans un milieu acousto-élastique non homogène. On cherche à déterminer la présence d'inclusions élastiques à partir d'observations partielles et bruitées, enregistrées dans la partie acoustique du milieu. On dérive tout d'abord une formulation variationnelle acousto-élastique des équations, puis on construit un solveur élément finis, pour résoudre numériquement les problèmes direct et retourné temporellement. En s'inspirant de travaux sur la migration sismique, on introduit un critère objectif, qui nous permet de construire une image des inclusions a déterminer. Des illustrations numériques, sur des données qui simulent la configuration du cancer du sein, sont proposées et montrent qu'il est possible de différencier des inclusions, même avec des propriétés différentes.

* Corresponding author.
E-mail addresses: franckassous55@gmail.com (F. Assous), moshelin1@walla.co.il (M. Lin).

https://doi.org/10.1016/j.crme.2019.02.001
1631-0721/

Version française abrégée

Le retournement temporel est un thème qui fait l'objet de recherches très actives depuis plus de deux décennies. De nombreuses équipes travaillent actuellement sur ce sujet, tant d'un point de vue théorique, physique que numérique. Il a été initialement développé expérimentalement par Mathias Fink en 1992 en acoustique et a montré des caractéristiques très intéressantes [1].

Le principe de base du retournement temporel est la propriété de réversibilité des phénomènes de propagation d'ondes dans des milieux non dissipatifs. Par conséquent, on peut rétropropager – c'est à dire inverser le sens du temps – de signaux émis en les laissant se propager jusqu'à l'emplacement de la source ou des objects diffractants qui les ont générés. L'expérience initiale, proposée par Mathias Fink, consistait à refocaliser très précisément un signal enregistré après qu'il ait traversé une barrière constituée de barres métalliques disposées de façon aléatoire.

D'un point de vue théorique, en tant que problème inverse, la méthode de retournement temporel, résolue dans des circonstances idéales, devrait pouvoir redonner la solution exacte. En pratique, cependant, on est confronté à un manque d'informations (bruit de mesure, données partielles en espace et en temps, manque de connaissances des propriétés du milieu, de la source, etc.).

Dans cette Note, on se propose d'étendre la méthode du retourné temporel en considérant un milieu acousto-élastique non homogène. Dans une première partie, on dérive une formulation variationnelle acousto-élastique des équations, puis on construit un solveur élément finis, pour résoudre numériquement le problème direct et le problème retourné temporellement.

Nous introduisons ensuite un critère inspiré de la migration sismique, et nous appliquons notre méthode pour identifier ou différencier deux inclusions proches, ayant éventuellement des propriétés élastiques différentes, dont les caractéristiques élastiques correspondent à des tumeurs du sein de type bénin et malin.

Pour des raisons de simplicité, nous avons considéré un milieu « stratifié ». Nous avons déterminé la présence d'inclusions dans la partie élastique, et ce, uniquement à partir des ondes acoustiques enregistrées par la ligne de récepteurs située dans la partie fluide du milieu. Enfin, pour être plus proche de cas réels, nous avons supposé que cette ligne de récepteurs a une ouverture partielle, c'est-à-dire n'entoure pas la totalité du domaine où se situent les inclusions à imager, et que les données disponibles sont bruitées.

1. Introduction

Time reversal (TR) has been a subject of very active research for over two decades. Many international teams are currently working on the subject from theoretical, physical, and numerical points of view. It was originally experimentally developed by Mathias Fink in 1992 in acoustics and showed very interesting features [1].

Time reversal is a procedure based on the reversibility property of wave propagation phenomena in non-dissipative media. As a consequence, one can "time-reverse" developed signals, by letting them propagate back in time to the location of the source (or scatterers) that emitted them originally. The initial experiment, proposed by Mathias Fink, was to refocus, very precisely, a recorded signal after passing through a barrier consisting of randomly distributed metal rods.

Theoretically, as well as an inverse problem solved in ideal circumstances, the TR method should yield the exact solution. However, there is always the possibility that under some (realistic!) conditions, the time-reversed process will fail. This may happen due to several reasons: measurement noise, availability of only partial information in space or in time, and lack of knowledge about the properties of the medium.

Since Fink's experiment, numerous applications of this physical principle have been designed, in seismology, for locating the epicenter of an earthquake from measurements taken on the ground [2], and in medical imaging [3]. The first mathematical analysis can be found in [4] for a homogeneous medium and in [5], [6] for a random medium.

In this Note, we propose to extend the TR method by considering an acousto-elastic medium that will help us mimic, for example, breast tissue. We will apply our approach to identify an "inclusion", or to differentiate between two close inclusions, eventually with different elastic properties, corresponding to different breast tumors, for instance, benign and malignant. Typically, a benign tumor corresponds to normal breast tissues, with a Young modulus between 1 and 70 kPa, whereas malignant tumors have a Young modulus varying from 15 to 500 kPa (see, for instance, [7]).

Basically, the method consists first in solving a forward problem to create synthetic (namely simulated) data recorded by receivers. From these data, one will solve a time-reversed problem to compute a reversed field. Then, in the same spirit as in reversetime migration [8] or topological gradient methods [9], one will correlate these forward and backward responses in time to construct an imaging function. Using the intersection of these two wave fronts will help us determine the inclusion location and some of its properties.

In addition, to be closer to what happens in many real cases as in medical imaging and other fields, we do not assume that the line of receivers encloses the bounded domain Ω; we rather consider that the aperture is reduced, and that only noisy data are available. For the sake of simplicity, we will consider a "layered" medium, and we want to determine the presence of "inclusions" in the elastic part from recorded acoustic waves scattered by these inclusions. However, as pointed out, for instance, in [10], the method does not require *a priori* knowledge of the physical properties of the inclusions.

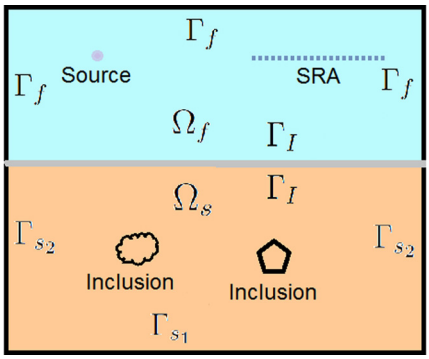

Fig. 1. Geometry of a fluid–solid domain Ω (example of 2D stratified medium), with the inclusions D and the source-receivers array (SRA) (dashed line).

2. The forward model

2.1. Setting of the problem

We consider an incident acoustic wave impinging on an inclusion D (which may contain one or several obstacles) characterized by different physical properties from the surrounding non-homogeneous medium. More precisely, an incident wave – generated by a known source or being an incoming wave "from infinity" – is propagated in a fluid medium, characterized by a known acoustic wave propagation velocity $V_{\rm f}^{\rm p} = \sqrt{\frac{\lambda_{\rm f}}{\rho_{\rm f}}}$, $\rho_{\rm f}$ and $\lambda_{\rm f}$ denoting respectively the density and the bulk modulus of the fluid. This wave is then transmitted (and partially reflected) into a solid medium, characterized by known wave propagation velocities $V_{\rm s}^{\rm p} = \sqrt{\frac{\lambda_{\rm s}+2\,\mu_{\rm s}}{\rho_{\rm s}}}$ and $V_{\rm s}^{\rm s} = \sqrt{\frac{\mu_{\rm s}}{\rho_{\rm s}}}$, $\rho_{\rm s}$ and $\lambda_{\rm s}$, $\mu_{\rm s}$ being respectively the density and the Lamé coefficients of the solid.

This wave is then scattered by one or several inclusions D located inside the solid domain, which each may contain several obstacles, inhomogeneities and nonlinearity. The resulting scattered wave is then recorded by a source-receivers array (SRA) located in the fluid part of the domain, denoted by $\Gamma_{\rm SRA}$ (see Fig. 1). We also assume that after a time $T_{\rm f}$, the total field is negligible in the domain of interest Ω.

To model this phenomenon, we consider the scalar wave equation in the fluid part $\Omega_{\rm f} \subset \Omega$, the elastodynamic wave equation in the solid part $\Omega_{\rm s} \subset \Omega$, together with interface transmission conditions. For the sake of simplicity, we will assume in what follows that the domain Ω is a bounded two-dimensional rectangular domain, that is $\Omega \subset \mathbb{R}^N$, $N = 2$, made of two layers $\Omega_{\rm f}$ and $\Omega_{\rm s}$. However, there is no "conceptual" difficulty to derive the same problem with several subdomains and a more complex geometry, or in a three-dimensional geometry.

More precisely, we introduce a two-dimensional fluid–solid domain $\Omega = \Omega_{\rm f} \cup \Omega_{\rm s}$ (see Fig. 1). We denote by $\partial\Omega_{\rm f}$ the boundary of $\Omega_{\rm f}$ and $\mathbf{n} = (n_1, n_2)$ is the unit outward normal vector to $\partial\Omega$. We denote by $p(\mathbf{x}, t)$ the pressure on a time t, $\mathbf{x} = (x_1, x_2) \in \Omega_{\rm f}$, and by $f(\mathbf{x}, t)$ a given source. In these conditions, the acoustic wave equation in $\Omega_{\rm f}$ is written as

$$\frac{1}{\lambda_{\rm f}}\frac{\partial^2 p}{\partial t^2} - \mathrm{div}\,(\frac{1}{\rho_{\rm f}}\nabla p) = f \tag{1}$$

together with homogeneous initial conditions at the initial time $t = 0$

$$p(t=0) = 0, \quad \frac{\partial p}{\partial t}(t=0) = 0 \tag{2}$$

We assume that the boundary $\partial\Omega_{\rm f}$ can be split in $\partial\Omega_{\rm f} = \Gamma_{\rm f} \cup \Gamma_I$, where Γ_I denotes the interface between the fluid and solid parts, assumed, to simplify the presentation, to be horizontal. We supplement Eqs. (1)–(2) with absorbing boundary conditions (ABC) [11] on $\partial\Omega_{\rm f}$,

$$\frac{\partial p}{\partial t} = -V_{\rm p}\,\nabla p \cdot \mathbf{n} \quad \text{on } \Gamma_{\rm f} \tag{3}$$

On the fluid–solid interface Γ_I, transmission conditions will be added, see (7) below.

Similarly, for the solid part $\Omega_{\rm s}$ of the domain, the velocity $\mathbf{u}(\mathbf{x}, t) = (u_1(x_1, x_2, t), u_2(x_1, x_2, t))$ at a point $\mathbf{x} = (x_1, x_2) \in \Omega_{\rm s}$ satisfies, for all $t > 0$,

$$\rho_{\rm s}\frac{\partial^2 u_i}{\partial t^2} - \sum_{j=1,2}\frac{\partial}{\partial x_j}\tau_{ij}(\mathbf{u}) = 0\,, \quad i = 1, 2 \tag{4}$$

where $\tau(\mathbf{u}) := (\tau_{ij}(\mathbf{u}))_{1\le i,j\le 2}$ is the (time derivative of the) classical stress matrix defined by

$$\tau_{11}(\mathbf{u}) = \lambda_s \mathrm{div}\,\mathbf{u} + 2\mu_s \frac{\partial u_1}{\partial x_1}, \quad \tau_{12}(\mathbf{u}) = \tau_{21}(\mathbf{u}) = \mu_s\left(\frac{\partial u_1}{\partial x_2} + \frac{\partial u_2}{\partial x_1}\right), \quad \tau_{22}(\mathbf{u}) = \lambda_s \mathrm{div}\,\mathbf{u} + 2\mu_s \frac{\partial u_2}{\partial x_2}$$

This equation is supplemented with homogeneous initial conditions

$$\mathbf{u}(t=0) = 0, \quad \frac{\partial \mathbf{u}}{\partial t}(t=0) = 0 \tag{5}$$

Assuming that the boundary $\partial\Omega_s$ can be split in $\partial\Omega_s = \Gamma_s \cup \Gamma_I$, these equations are also supplemented with absorbing boundary conditions on Γ_s, as proposed in [12],

$$\mathbb{A}\frac{\partial \mathbf{u}}{\partial t} = \mathbb{T}(\mathbf{u})\,\mathbf{n} \tag{6}$$

where the matrix $\mathbb{A}$ is a diagonal $N \times N$ matrix, with $A_{11} = -\sqrt{\rho_s(\lambda_s + 2\mu_s)}$, $A_{22} = -\sqrt{\rho_s \mu_s}$ for horizontal boundaries Γ_{s_1}, and the contrary for vertical boundaries Γ_{s_2}. A general expression of $\mathbb{A}$ can be found in [12] for more complex geometries of the boundary.

Finally, on the interface Γ_I, we impose the continuity of the normal component

$$\frac{1}{\rho_f}\frac{\partial p}{\partial \mathbf{n}} = \frac{1}{\rho_f}\nabla p \cdot \mathbf{n} = -\frac{\partial \mathbf{u}}{\partial t} \cdot \mathbf{n} \tag{7}$$

where $\mathbf{n}$ denotes here the unit outward normal vector from $\partial\Omega_s$ to $\partial\Omega_f$.

For an horizontal interface, this can be simply expressed as $\frac{1}{\rho_f}\frac{\partial p}{\partial x_2} = -\frac{\partial u_2}{\partial t}$. We also impose the continuity of the normal component of the stress tensor.

$$\frac{\partial p}{\partial t} n_i = \sum_{j=1,2} \tau_{ij}(\mathbf{u})\, n_j, \quad i = 1, 2 \tag{8}$$

Here again, this is simply expressed for an horizontal interface

$$0 = \frac{\partial u_1}{\partial x_2} + \frac{\partial u_2}{\partial x_1}, \quad \frac{\partial p}{\partial t} = \lambda_s \frac{\partial u_1}{\partial x_1} + (\lambda_s + 2\mu_s)\frac{\partial u_2}{\partial x_2}$$

In other words, there is conservation of $N + 1 = 3$ scalar quantities. Note also that these conditions appear as *natural boundary conditions* in the variational formulation that will be derived below, due to the use of the pressure–velocity formulation, Eqs. (1)–(4).

2.2. Variational formulation

We now introduce the variational formulation for the acousto-elastodynamics equations. Let q be a test function for acoustic wave equation, which belongs to the *ad hoc* Sobolev space[1] V, and $\mathbf{v} = (v_1, v_2)$ a vector test function for the elastodynamics wave equation, which also belongs to the relevant vector Sobolev space $\mathbf{V}$. Multiplying (1) by $q \in V$, integrating over the domain Ω_f, and using integration by parts, we get

$$\int_{\Omega_f} \frac{1}{\lambda_f}\frac{\partial^2 p}{\partial t^2} q \,\mathrm{d}\omega + \int_{\Omega_f} \frac{1}{\rho_f}\nabla p \cdot \nabla q \,\mathrm{d}\omega - \int_{\partial\Omega_f} \frac{1}{\rho_f}\frac{\partial p}{\partial \mathbf{n}} q \,\mathrm{d}\sigma = \int_{\Omega_f} f q \,\mathrm{d}\omega \tag{9}$$

On the part Γ_I of the boundary $\partial\Omega_f$, we use the continuity of the normal component (7), and the ABC (3) on the part Γ_f. We get

$$\int_{\Omega_f} \frac{1}{\lambda_f}\frac{\partial^2 p}{\partial t^2} q \,\mathrm{d}\omega + \int_{\Omega_f} \frac{1}{\rho_f}\nabla p \cdot \nabla q \,\mathrm{d}\omega + \int_{\Gamma_I} \frac{\partial \mathbf{u}}{\partial t} \cdot \mathbf{n}\, q \,\mathrm{d}\sigma + \int_{\Gamma_f} \frac{1}{\sqrt{\rho_f \lambda_f}}\frac{\partial p}{\partial t} q \,\mathrm{d}\sigma = \int_{\Omega_f} f q \,\mathrm{d}\omega \tag{10}$$

Similarly to deriving the variational formulation in Ω_s, we use Green's identity (see [13], p. 288),

$$-\int_{\Omega_s} \mathrm{div}\,\mathbb{S} \cdot \mathbf{v} \,\mathrm{d}\omega = \int_{\Omega_s} \mathbb{S} : \nabla \mathbf{v} \,\mathrm{d}\omega - \int_{\partial\Omega_s} (\mathbb{S}\,\mathbf{n}) \cdot \mathbf{v} \,\mathrm{d}\sigma\,, \quad \forall \mathbf{v} \in \mathbf{V} \tag{11}$$

where $\mathbb{S}$ denotes a symmetric tensor field and the symbol: stands for the contracted product of two tensors. Multiplying (4) by $\mathbf{v} = (v_1, v_2) \in \mathbf{V}$, integrating over the domain Ω_s, and using integration by parts (11), we get

[1] classically, q belongs to the classical $H^1(\Omega)$ Sobolev space.

$$\int_{\Omega_s} \rho_s \frac{\partial^2 \mathbf{u}}{\partial t^2} \cdot \mathbf{v}\, d\omega + \int_{\Omega_s} \lambda_s \mathrm{div}\,\mathbf{u}\, \mathrm{div}\,\mathbf{v}\, d\omega + \int_{\Omega_s} 2\mu_s \tau_{ij}(\mathbf{u})\, \tau_{ij}(\mathbf{v})\, d\omega - \int_{\partial\Omega_s} \tau_{ij}(\mathbf{u})\, v_i\, n_j\, d\sigma = 0 \tag{12}$$

Using now the continuity of the normal component of the stress tensor (8) on the interface and the ABC (6) on Γ_s, we obtain

$$\int_{\Omega_s} \rho_s \frac{\partial^2 \mathbf{u}}{\partial t^2} \cdot \mathbf{v}\, d\omega + \int_{\Omega_s} \lambda_s \mathrm{div}\,\mathbf{u}\, \mathrm{div}\,\mathbf{v} + 2\mu_s \tau_{ij}(\mathbf{u})\, \tau_{ij}(\mathbf{v})\, d\omega - \int_{\Gamma_I} \frac{\partial p}{\partial t}\, \mathbf{v}\cdot\mathbf{n}\, d\sigma - \int_{\Gamma_s} \mathbb{A} \frac{\partial \mathbf{u}}{\partial t} \cdot \mathbf{v}\, d\sigma = 0 \tag{13}$$

Remark 1. The transmission conditions at the interface Γ_I appear through an anti-symmetric form $c(\cdot,\cdot)$ defined by

$$\frac{d}{dt} c((p,\mathbf{u}),(q,\mathbf{v})) := \frac{d}{dt}\left(\int_{\Gamma_I} -p\,\mathbf{v}\cdot\mathbf{n}\, d\sigma + \int_{\Gamma_I} \mathbf{u}\cdot\mathbf{n}\, q\, d\sigma \right)$$

This allows us to define an energy of the system and to prove that this energy is conserved, in the absence of ABC, or decreases, in the presence of ABC.

3. Recreate the past *via* time reversal

Our aim is to reconstruct the time-reversed wave, denoted by $(p_R, \mathbf{u}_R)$, scattered by an inclusion D, which may contain several obstacles or inhomogeneities, from the measurements on the receiver array Γ_{SRA}, the *incident* wave being known. In our case, due to the non-homogeneity of the fluid–solid domain, made of two layers at least, we define the *incident* field as the pressure–velocity fields that propagate in the absence of scatterer D. This assumes that the location of the interface Γ_I and of the possible other discontinuities is known. The recording being performed in the fluid part, we have likewise to solve a time-reversed fluid–solid problem from acoustic recording, that is, from the measurement of the pressure p in the fluid part, more precisely on Γ_{SRA}. More generally, the recorded data can be either modeled by a boundary condition, as for example in [14], or *via* a right-hand side with a support on Γ_{SRA}. We chose here the second option, since the SRA are located inside the computational domain, and not on a boundary.

For this purpose, we derive a boundary value problem whose solution is $(p_R, \mathbf{u}_R)$ in $\Omega = \Omega_f \cup \Omega_s$. We know neither the physical properties nor the exact location of the inclusion D. The only things we know are the physical properties of the surrounding medium. Examples of time-reversal techniques (numerical or experimental) can be found in [1,10,14–16].

For the acoustic part of the domain Ω_f, we denoted by $p^R(\mathbf{x}, t')$ the time-reversed pressure, defined by $p^R(\mathbf{x}, t') = p(\mathbf{x}, T_f - t)$, $\mathbf{x} \in \Omega_f$, T_f denoting the final time. Since the wave equation involves only second-order time derivatives, this definition ensures that the reverse field $p^R(\mathbf{x}, t')$ is a solution to the acoustic wave equation

$$\frac{1}{\lambda_f} \frac{\partial^2 p^R}{\partial t'^2} - \mathrm{div}\left(\frac{1}{\rho_f} \nabla p^R\right) = f_{SRA} \tag{14}$$

where f_{SRA} denotes the time reversal of the fields recorded on Γ_{SRA}, namely $f_{SRA}(t') = p(T_f - t)_{|_{SRA}}$. This equation is supplemented with (TR) initial conditions and (TR) absorbing boundary conditions on Γ_f, time-reversed analogous to (2) and (3).

Similarly, we also introduce the elastic time-reversed problem associated with Eq. (4). We denote by $\mathbf{u}^R(\mathbf{x}, t') = (u_1^R(x_1, x_2, t'), u_2^R(x_1, x_2, t'))$ the time-reversed velocity solution to linear elastodynamics, which solves

$$\rho_s \frac{\partial^2 u_i^R}{\partial t'^2} - \sum_{j=1,2} \frac{\partial}{\partial x_j} \tau_{ij}(\mathbf{u}^R) = 0\,, \quad i = 1, 2 \tag{15}$$

$(\tau_{ij}(\mathbf{u}^R))_{1\le i,j\le 2}$ being defined as $(\tau_{ij}(\mathbf{u}))_{1\le i,j\le 2}$ in the forward problem, together with (TR) initial conditions, and (TR) absorbing boundary conditions on Γ_s, with expressions analogous to (5) and (6).

Finally, we derive the time-reversed continuity transmission conditions at the interface Γ_I

$$\frac{1}{\rho_f} \frac{\partial p^R}{\partial \mathbf{n}} = \frac{\partial \mathbf{u}^R}{\partial t'} \cdot \mathbf{n}\,, \text{ namely } \frac{1}{\rho_f} \frac{\partial p^R}{\partial x_2} = \frac{\partial u_2^R}{\partial t'} \text{ for an horizontal interface} \tag{16}$$

$$-\frac{\partial p^R}{\partial t'} n_i = \sum_{j=1,2} \tau_{ij}(\mathbf{u}^R)\, n_j, \quad i = 1, 2 \tag{17}$$

expressed in our case as

$$\frac{\partial u_1^R}{\partial x_2} + \frac{\partial u_2^R}{\partial x_1} = 0, \qquad -\frac{\partial p^R}{\partial t'} = \lambda_s \frac{\partial u_1^R}{\partial x_1} + (\lambda_s + 2\mu_s) \frac{\partial u_2^R}{\partial x_2} \tag{18}$$

3.1. Variational formulation

We follow the same principles as for the forward problem (see subsection 2.2) to derive the variational formulation for the time-reversed acousto-elastic equations. For completeness, we present below the expression finally obtained, which is written

$$\int_{\Omega_f} \frac{1}{\lambda_f} \frac{\partial^2 p^R}{\partial t'^2} q \, d\omega + \int_{\Omega_f} \frac{1}{\rho_f} \nabla p^R \cdot \nabla q \, d\omega - \int_{\Gamma_I} \frac{\partial \mathbf{u}^R}{\partial t'} \cdot \mathbf{n} \, q \, d\sigma - \int_{\Gamma_f} \frac{1}{\sqrt{\rho_f \lambda_f}} \frac{\partial p^R}{\partial t'} q \, d\sigma = \int_{\Gamma_{SRA}} f_{SRA} \, q \, d\omega \tag{19}$$

$$\int_{\Omega_s} \rho_s \frac{\partial^2 \mathbf{u}^R}{\partial t'^2} \cdot \mathbf{v} \, d\omega + \int_{\Omega_s} \lambda_s \operatorname{div} \mathbf{u}^R \operatorname{div} \mathbf{v} + 2 \mu_s \tau_{ij}(\mathbf{u}^R) \tau_{ij}(\mathbf{v}) \, d\omega + \int_{\Gamma_I} \frac{\partial p^R}{\partial t'} \mathbf{v} \cdot \mathbf{n} \, d\sigma + \int_{\Gamma_s} \mathbb{A} \frac{\partial \mathbf{u}^R}{\partial t'} \cdot \mathbf{v} \, d\sigma = 0 \tag{20}$$

This formulation and the forward one, Eqs. (10)–(13), are discretized by similar numerical schemes. Both are approximated by using a P_2 finite element method with FreeFem++ [17]. The time derivative is approximated by a second-order centered finite difference scheme, which is time reversible also on the numerical level.

4. Numerical results

The aim of the method is now to identify the presence and some elastic properties of unknown inclusions. From a numerical point of view, it involves three stages of computation.

(i) First, we have to create the synthetic data by solving the forward problem to record the value of the pressure p on Γ_{SRA}. The incident field $\mathbf{u}^I(t, \mathbf{x})$, introduced in Section 3, will be also computed in this first step, to enable construction of the scattered field from the total one by subtraction.

(ii) From these recorded data, one compute the reversed field by solving the time-reverse formulation in the entire domain Ω, assuming that there is no inclusion.

(iii) The last step consists in imaging the unknown scatterers in the medium, responsible of the diffraction of the incident wave. To this purpose, we introduce a correlation method between the forward incident wave $\mathbf{u}^I$, and the reversed scattered wave $\mathbf{u}_R^S$, in the same spirit as in the case of those involved, for instance, in reverse-time migration. There is a plethora of references on this subject, particularly in the context of geophysics modeling and inversion (see, among others, [18] or [8]), where the adjoint-solution formulation can be viewed as a particular TR problem, cf. [10]). The principle consists in correlating the forward and backward responses in time. Indeed, clear refocusing at the true location of the source is obtained as an intersection of these two wave fronts. Hence, we have considered the following criterion:

$$RTM(\mathbf{x}) = \int_{t=0}^{t=T_f} \mathbf{u}_R^S(T_f - t, \mathbf{x}) \cdot \mathbf{u}^I(t, \mathbf{x}) \, dt \tag{21}$$

Criterion (21) can also be viewed as an imaging functional, similar to those arising from topological derivative-based methods, as described in [9,19,20]. Note also that analogous criteria can be defined using, for instance, only one component u_x, u_y, or the div or curl operators. In the same way, one could also consider criteria based on mathematical energies, that can be viewed as the L^2 (without including the gradients) or H^1 (with the gradients) norms.

To illustrate the usefulness of the method described above, we present numerical results obtained for the scatterer identification problem in the case of a medium with elastic properties that mimic a breast tissue. We have first to solve the forward problem and to record the value of the pressure p on Γ_{SRA}. For this purpose, an incident wave is generated by a point source located in the fluid part (the right-hand side of (1)), such that after a time T_f the total field is almost negligible. The SRA is an horizontal line including 55 sensors, see for example Fig. 1. For the fluid part, we choose $\rho = 1000$ kg/m^3 and $\lambda = 2.25$ GPa, that is a velocity $V_p = 1500$ m/s. For the solid part, we choose $\rho = 1000$ kg/m^3, $\lambda = 1.83$ GPa and $\mu = 18.33$ kPa, which corresponds to plane and shear wave velocities $V_p = 1354.02$ m/s and $V_s = 4.28$ m/s. The simulation will run during a total time $T_f = 130$ µs, with a time step $\Delta t = 1$ µs.

There are two inclusions in our simulations with different sizes and shapes (both of them are not circles but ellipses), and elastic properties. The one that represents a benign tumor is such that $\rho = 1000$ kg/m^3, $\lambda = 2.16$ GPa and $\mu = 21.66$ kPa, which corresponds to plane and shear wave velocities $V_p = 1471.97$ m/s and $V_s = 4.65$ m/s. To simulate a malignant tumor, we use $\rho = 1000$ kg/m^3, $\lambda = 3.33$ GPa and $\mu = 33.33$ kPa, which correspond to plane and shear wave velocities $V_p = 1825.75$ m/s and $V_s = 5.77$ m/s. Note that both inclusions are penetrable, which means that the reflection of the incident wave highlighting the inclusion is quite weak.

The source used to generate the acoustic wave in the fluid part is a Ricker function of the form $f(\mathbf{x}, t) = (1 - 2\pi^2(\nu_0 t - 1)^2) \, e^{-\pi^2(\nu_0 t - 1)^2}$, with a central frequency $\nu_0 = 100$ kHz and a corresponding wavelength equal to $\lambda_W = 12$ mm.

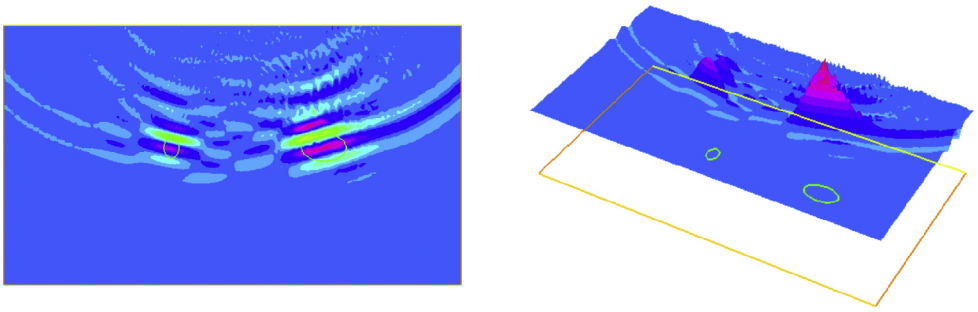

Fig. 2. 2D (left) and 3D (right) representation of the imaging function (21) in Ω_s for two malignant scatterers, with a level of noise of 10%.

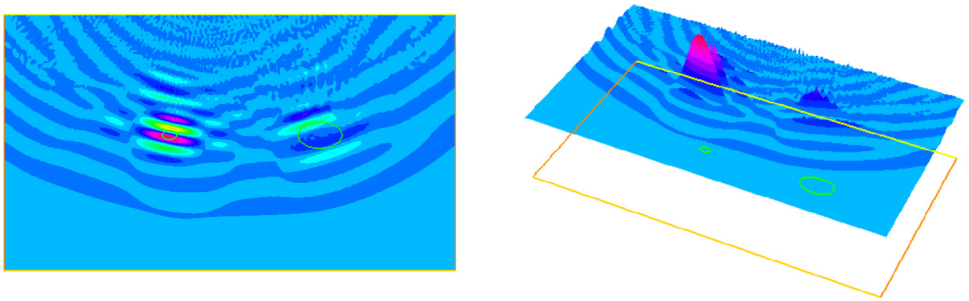

Fig. 3. 2D (left) and 3D (right) representation of the imaging function (21) in Ω_s for a small malignant scatterer (left), and a benign one (right), with a level of noise of 10%.

To verify the (in)sensitivity of the method with respect to the noise in the data, we added Gaussian noise to the recorded field p^S with

$$p^S_{\text{Noise}} = (1 + Coeff * randn) * p^S$$

where *randn* satisfies a centered reduced normal law and *Coeff* is the noise level, taken equal to 10% in our simulations. As mentioned above, the knowledge of the source (usual in PDE-constrained optimization problems) allows us to compute the incident wave, from which the scattered field can be obtained from the total field by subtraction. Remark also that this is a multiplicative, and non an additive noise. Indeed, following [21], this allows us to disturb the registered signal avoiding "inverse crime" related to the interaction between the numerical schemes used for the forward and the reverse problem. In other words, this is a way to model the noise due to the recording device, and does not represent a background noise, that will be rather modeled by an additive noise.

Then the TR formulation is solved in the entire domain Ω, assuming that there are no inclusions, by approximating numerically Eqs. (19)–(20). In addition to the added noise, to avoid any inverse crime (see [16]), the solution to the reverse problem is performed in a mesh different from the one uses for solving the forward one. We finally compute the imaging functional $RTM(\mathbf{x})$ defined by (21).

For the purpose of illustration, we consider a two-layered medium, made of fluid part (top) and of a elastic one (bottom), the elastic part sketching a breast tissue geometry. Hence, the scatterers are illuminated by an incident acoustic field, which is first transmitted to the elastic medium through the interface Γ_I, and then scattered by the inclusions, before to be recorded by the SRA. The SRA being located in the fluid part, they are able to record only a scalar quantity (the pressure $p(\mathbf{x}, t)$), and not a vector velocity $\mathbf{u}(\mathbf{x}, t)$.

We consider the two following configurations. In the first one, see Fig. 2, two malignants scatterers with different size D_1, D_2, separated by a distance of around $3\lambda_W$ are considered. The size of D_1 is $2/3\lambda_W$, and the size of D_2 is equal to $3/4\lambda_W$. In this figure, we plot the value of the function RTM defined in Eq. (21), in the elastic layer. The left part represents a 2D view, whereas on the right part the same image is depicted in a 3D view. This clearly shows that one is able to determine the existence and location of the two malignant tumors. We have also performed the same numerical tests with added noise on the total field, instead of the scattered one: the results are nearly the same. This is not a surprise, since it has been proved that time-reverse methods are fairly insensitive to noise in the data (see for instance [14,22]).

In the second numerical test, we are interested in testing the robustness of this method, by considering only one malignant scatterer D_1 on the left, and a benign one D_2 on the right part. In addition, in that case, we reduce the size of the malignant object to check how we can detect it. As one can see in Fig. 3, here again, one is able to clearly distinguish the two inclusions, and also to determine, at least qualitatively, that the left one is probably malignant, whereas the right one is benign. The definition of more quantitative criteria to determine the presence and the properties of these inclusions is the subject of our future work.

5. Conclusion

In this Note, we proposed a time-reversal method for coupled acousto-elastic non-homogeneous wave equations. A finite element method, derived from a variational formulation, was also presented. We show that one can locate the position of obstacles in the elastic parts, even in the presence of partial and noisy information, from acoustic data recorded in the fluid part of the domain. By cross-correlating the incident field with the time-reversed scattered field, we were able to determine the properties of these inclusions and to differentiate two close inclusions, even with different elastic properties. We present promising numerical results and options for further development.

References

[1] M. Fink, F. Wu, D. Cassereau, R. Mallart, Imaging through inhomogeneous media using time reversal mirrors, Ultrason. Imag. 13 (2) (1991) 179–199.
[2] C. Larmat, J.-P. Montagner, M. Fink, Y. Capdeville, A. Tourin, E. Clévédé, Time-reversal imaging of seismic sources and application to the great sumatra earthquake, Geophys. Res. Lett. 33 (2006) 1–4.
[3] Y.K. Tan, M. Ostergaard, P.G. Conaghan, Imaging tools in rheumatoid arthritis: ultrasound vs magnetic resonance imaging, Rheumatology 51 (2012) 36–42.
[4] C. Bardos, M. Fink, Mathematical foundations of the time reversal mirror, Asymptot. Anal. 29 (2002) 157–182.
[5] J.-F. Clouet, J.-P. Fouque, A time-reversal method for an acoustical pulse propagating in randomly layered media, Wave Motion 25 (1997) 361–368.
[6] P. Blomgren, G. Papanicolaou, H. Zhao, Super-resolution in time-reversal acoustics, J. Acoust. Soc. Am. 111 (2002) 230–248.
[7] E. Fernandez, Breast elastography: present and future, Int. J. Radiol. Radiat. Ther. 4 (3) (2017) 379–384.
[8] J.F. Claerbout, Imaging the Earth's Interior, Blackwell, 1985.
[9] N. Dominguez, V. Gibiat, Y. Esquerré, Time domain topological gradient and time reversal analogy: an inverse method for ultrasonic target detection, Wave Motion 42 (2005) 31–52.
[10] F. Assous, M. Kray, F. Nataf, Time-reversed absorbing conditions in the partial aperture case, Wave Motion 49 (2012) 617–631.
[11] R. Clayton, B. Engquist, Absorbing boundary conditions for acoustic and elastic wave equations, Bull. Seismol. Soc. Am. 67 (6) (1977) 1529–1540.
[12] A. Bamberger, P. Joly, J. Roberts, J.L. Teron, Absorbing Boundary Conditions for Rayleigh Waves, Research Report RR-0384, INRIA, 1985.
[13] P.G. Ciarlet, Mathematical Elasticity, Volume I: Three-Dimensional Elasticity, Series Studies in Mathematics and Its Applications, North-Holland, Amsterdam, 1988.
[14] F. Assous, M. Kray, F. Nataf, E. Turkel, Time reversed absorbing condition: application to inverse problems, Inverse Probl. 27 (6) (2011) 065003.
[15] P. Kosmas, C.M. Rappaport, Time reversal with the FDTD method for microwave breast cancer detection, IEEE Trans. Microw. Theory Tech. 53 (7) (2005) 2317–2323.
[16] D. Givoli, E. Turkel, Time reversal with partial information for wave refocusing and scatterer identification, Comput. Methods Appl. Mech. Eng. 213 (216) (2012) 223–242.
[17] F. Hecht, New development in FreeFem++, J. Numer. Math. 20 (3–4) (2012) 251–265.
[18] A.J. Berkhout, Seismic Migration, Elsevier, Amsterdam, Oxford, New York, Tokyo, 1984.
[19] E. Bachmann, X. Jacob, S. Rodriguez, V. Gibiat, Three-dimensional and real-time two-dimensional topological imaging using parallel computing, J. Acoust. Soc. Am. 138 (2015) 1796.
[20] M. Bonnet, Topological sensitivity for 3D elastodynamic and acoustic inverse scattering in the time domain, Comput. Methods Appl. Mech. Eng. 195 (2006) 5239–5254.
[21] D.L. Colton, R. Kress, Inverse Acoustic and Electromagnetic Scattering Theory, Applied Mathematical Sciences Series, Springer, 2013.
[22] I. Levi, E. Turkel, D. Givoli, Time reversal for elastic wave refocusing and scatterer location recovery, J. Comput. Acoust. 23 (2015) 1–29.